IEEE Access
Multidisciplinary ⋮ Rapid Review ⋮ Open Access Journal

Received October 9, 2020, accepted October 23, 2020, date of publication October 28, 2020, date of current version November 11, 2020.

Digital Object Identifier 10.1109/ACCESS.2020.3034459

A Novel Polar Rapid Transfer Alignment for Shipborne SINS Under Arbitrary Misalignments

JIANHUA CHENG, JING CAI, ZHENMIN WANG, AND JIAXIN LIU
College of Intelligent Systems Science and Engineering, Harbin Engineering University, Harbin 150001, China

Corresponding author: Jing Cai (sunny_93cj@sina.com)

This work was supported in part by the National Natural Science Foundation of China under Grant 61633008, Grant 61773132, and Grant 61803115; in part by the 7th Generation Ultra Deep Water Drilling Unit Innovation Project sponsored by Chinese Ministry of Industry and Information Technology; in part by the Heilongjiang Province Science Fund for Distinguished Young Scholars under Grant JC2018019; and in part by the Fundamental Research Funds for Central Universities under Grant HEUCFP201768.

ABSTRACT The traditional polar rapid transfer alignment (RTA) are generally modeled under small angle misalignment assumption. Those linearized and nonlinear polar RTA error models presented, so far, are not capable of accurately representing the nonlinear properties of the system where the all-orientation large attitude errors happen between the master and slave strap-down inertial navigation systems (SINS). It cannot satisfy the accuracy for the SINS initialization and has a singularity in computation. In this article, the misalignment quaternion in the grid frame was selected as the state and observation. An innovative polar RTA algorithm using the quaternion matching and the augmented unscented Kalman filter (UKF) was then proposed to estimate all-orientation large attitude misalignments in polar regions. Furthermore, the associated error propagation equations were redesigned in the grid frame and with compensations for the lever-arm effect. The augmented UKF model was further adjusted to apply. Simulation and semi-physical experiment results demonstrated that the performance of the innovative polar RTA algorithm proposed here outperformed those via traditional polar RTA techniques, especially with 3-axis large-angle misalignments, and was even robust with the disturbance of lever-arm effect aggravated by the harsh polar environment.

INDEX TERMS Large attitude misalignments, polar regions, quaternion, rapid transfer alignment, SINS.

I. INTRODUCTION

The rapid melting of glaciers caused by global warming has probably rendered marine vessels voyage across the north pole, significantly minimizing the time sailing along the Asia-Europe route. Thereby, the north polar region has growingly become a hotly disputed and scrabbled region since it abounds with the biological and mineral resources and occupies a strategic position [1]. Among various navigation techniques [2], the strapdown inertial navigation system (SINS) is a priority with its superior concealment, autonomy, which is seldom affected by the environment and outputs all-navigation information [3], [4]. To achieve a fast and accurate initialization, the rapid transfer alignment (RTA) is a primary alignment technique for the moving base [5]–[7]. However, the traditional error model of RTA is constructed under the geographic frame. This mechanism inevitably happens to magnify errors along latitudes and overflow in the calculation [8].

To solve these problems, the grid frame [10] replaced the traditional geographical north by the Greenwich meridian as a reference for the definition of heading. The mechanism of polar RTA was necessarily re-derived under the grid frame for a high-precision alignment, whereas it merely applied to the infinitesimal attitude misalignments [9]. In practice, the salve SINS of the equipped devices (e.g., vessel-carried weapons) located relative to the master reference even happens to almost 60° misalignments [11]. Thus, the polar RTA model for a large azimuth misalignment was developed with the premise of small horizontal attitude errors [12]. Due to the long-time insolation and the severe state of the sea, the deck deformation can reach 1 degree. The roll and pitch misalignment relative to the master reference even reach 10 degrees. In this situation, the system error model cannot be assumed using the infinitesimal angle assumption. Thereby, the nonlinear model and the associated filter algorithm require to be reconstructed and improved.

The associate editor coordinating the review of this manuscript and approving it for publication was Min Wang.

More recently, several parameterizations have been used as attitude representations, such as Euler angle [11], [13], cosine direction matrix (CDM) [14], rotation vector [15], and quaternion [16]–[19]. In detail, [11] constructed Ψ-angle error model, whereas [13] pointed out that this model still assumed horizontal attitude errors to small angles. The attitude matrix is generally inferred by rotating an orthogonal frame three times in an assigned sequence. This transformation matrix is inevitably composed of trigonometric functions whose nature is nonlinearity. Especially for weapons arbitrarily placed on deck, attitude along each axis may be significantly large relative to the master system, and complicated trigonometric functions are unavoidable in operations. The CDM was adopted in [14], yet only 3 degrees of freedom existed, that is, redundant six elements might increase the computational burden. Besides, CDM is a three-order polynomial of trigonometric functions of Euler angles. Its differential equation for nonlinear RTA is at least 6-order polynomial or more in [26], which is complex and singular in computation. The rotation vector was introduced in [15] to simplify the calculation, but the attitude error model was still adapted from the additive quaternion error model. Thus, the quaternion has been widely applied due to its non-singularity, all-orientation attitude representation, high precision, and simple computation [20]. Quaternions were used to construct an error propagation model in the computer frame approach, solving the initial attitudes uncertainty without an assumption of infinitesimal misalignments [16]. The additive and multiplicative quaternion errors were modeled for RTA in the low and medium latitudes [17]. Its simulation demonstrated that the z-axis misalignment converged as fast and precisely as horizontal attitude errors. Inspired by [17], Dai *et al.* established the nonlinear RTA model via multiplicative quaternions errors [18], proving that it is equivalent to the conventional small-angle linear model proposed in [5]. Given the highly nonlinear quaternion-based models, the manipulation and management of the quaternion measurement equation in [19] led to a linear pseudo-measurement equation, whereas its model neglected the lever-arm effect and was sensitive to flexural deformation. Overall, any linearization for improving precision and simplifying complexity must be abandoned, and all the disturbance should be considered, which may occur in polar regions.

To accommodate the polar RTA under 3-axis large misalignments, we need to develop a proper error model and adopt a suitable observation indispensably. In this article, the proposed algorithm adopts the misalignment quaternion in the grid frame as the state and observation to solve 3-axis large misalignments and rederives quaternion-based error models without any infinitesimal angle assumptions to supply a superior and feasible alignment for polar regions. This method relatively lowers the polynomial order and reduces the nonlinearity. We also consider the lever-arm effect and flexural deformation comprehensively and add to the proposed model. Furthermore, the measurement misalignment quaternion, in which the master attitude quaternions multiplies the slave one jointly, is directly used as an attitude observation to make the measurement equation more linear, avoiding the linearized error. Since the attitude representation in differential equations substitutes the Euler angle with the quaternion, the polynomial order is reduced from 6 to 2. However, the model is still nonlinear. An appropriate nonlinear estimator is required to process the quaternion-based system error model under arbitrary and inaccurate attitude error angles in polar regions.

We can use the extended Kalman filter (EKF), unscented Kalman filter (UKF), and particle filter (PF) to estimate nonlinear states. However, the PF comprises an enormous amount of calculations. The EKF was used for nonlinear RTA models in [21]. However, the EKF models are expanded using Jacobians, and the implementation difficulty of Jacobians is one shortcoming of the EKF [16]. A rapid transfer alignment based on the UKF was proposed in [22]. The UKF can reach higher accuracy, its performance outperforms those via EKF, and anti-interfere with a large initial error of states [23]. Nevertheless, the states and observations are multiplied by the quaternion-based noise in both system and measurement equations, and the UKF scarcely has a design of maintaining the normalization. Therefore, the augmented UKF [30], [31] is introduced here and adjusted to reasonably combine the prior state information with multiplicative noise influence. Enlighted by [24], [25], we adopt the projection to constrain the nonlinear-equation normalization, which means that the quaternion estimate was divided by its norm after each filtering directly.

The proposed polar RTA is verified and outperforms a conventional method [26] via the simulations and semi-physical experiments. Moreover, we omit the lever-arm model in the proposed model, intensify the noise, and become the simplified model as a comparison in simulations. The results illustrate that the proposed method is robust in the lever-arm effect. Conclusively, the contribution of this article is that the proposed algorithm can solve 3-axis large misalignments, achieve accurate RTA effectively, and anti-interfere the lever-arm effect intensified by the extreme environment in polar regions.

The outline of the reminder of this article is as follows. Firstly, the differential equations of error propagation involve the multiplicative attitude quaternion and velocity kinematics and are constructed under the grid navigation frame in Section II. In Section III, the dynamic and measurement models for the augmented UKF are further developed. A simulation system and semi-physical experiments are then designed, and the related results are shown in Section IV. The discussions aim at the mentioned results in Section V, and the conclusion is given in Section VI eventually.

II. ERROR PROPAGATION MODEL

The notation of frames that may be utilized in this article is listed at first:

i - the inertial frame;
e - the earth-centered-earth-fixed frame (ECEF);
n - the east-north-up navigation frame;

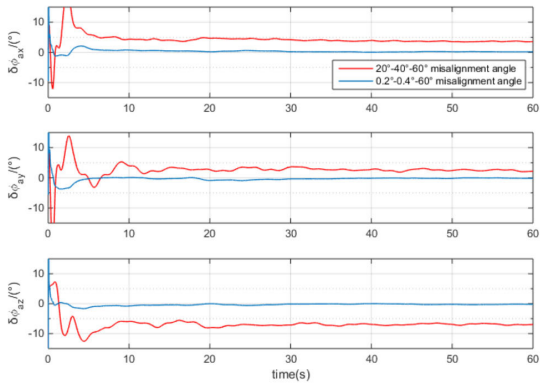

FIGURE 1. Navigation error curve for attitude at various horizontal misalignment angles.

G - the grid navigation frame;
m - the body frame of the master SINS;
s - the true body frame of the slave SINS;
s' -the computed body frame of the slave SINS.

A. MULTIPLICATIVE QUATERNION ERROR EQUATION

In the traditional polar rapid transfer alignment [26], ϕ_m^G represents the time-varying angular change between the master and slave CDM, known as the measurement misalignments. According to the Euler angle algorithm, the rotation rates $\omega_{ms'}^{s'}$ of the s′-frame relative to m-frame can be represented by the angular velocity of ϕ_m via rotating orthogonal frame three times in a specific sequence, which can be derived as

$$\begin{aligned}\omega_{ms'}^{s'G} &= \begin{bmatrix} \cos\phi_{my}^G & 0 & -\sin\phi_{my}^G \\ 0 & 1 & 0 \\ -\sin\phi_{my}^G & 0 & \cos\phi_{my}^G \end{bmatrix} \\ &\times \begin{bmatrix} 1 & 0 & 0 \\ 0 & \cos\phi_{mx}^G & \sin\phi_{mx}^G \\ 0 & -\sin\phi_{mx}^G & \cos\phi_{mx}^G \end{bmatrix} \begin{bmatrix} 0 \\ 0 \\ \dot{\phi}_{mz}^G \end{bmatrix} \\ &+ \begin{bmatrix} \cos\phi_{my}^G & 0 & -\sin\phi_{my}^G \\ 0 & 1 & 0 \\ -\sin\phi_{my}^G & 0 & \cos\phi_{my}^G \end{bmatrix} \begin{bmatrix} \dot{\phi}_{mx}^G \\ 0 \\ 0 \end{bmatrix} \\ &+ \begin{bmatrix} 0 \\ \dot{\phi}_{my}^G \\ 0 \end{bmatrix} \\ &= \begin{bmatrix} \cos\phi_{my}^G & 0 & -\cos\phi_{mx}^G\sin\phi_{my}^G \\ 0 & 1 & \sin\phi_{mx}^G \\ \sin\phi_{my}^G & 0 & \cos\phi_{mx}^G\cos\phi_{my}^G \end{bmatrix} \begin{bmatrix} \dot{\phi}_{mx}^G \\ \dot{\phi}_{my}^G \\ \dot{\phi}_{mz}^G \end{bmatrix} \end{aligned} \quad (1)$$

Assuming small horizontal angle misalignments (i.e., ϕ_{mx}^G and ϕ_{my}^G), the relation between $\omega_{ms'}^{s'}$ and ϕ_m can be inferred as $\omega_{ms'}^{s'G} = \dot{\phi}_m^G$. When the initial angle misalignment is respectively set to various values, the traditional polar RTA is simulated, and the attitude error curves at 85°N are shown in Fig.1.

The quantity ϕ_a^G in Fig.1 is the physical misalignment between the master and slave SINS, and the $\delta\phi_a$ is an error between the true and estimate misalignment to evaluate alignment performance. As shown in Fig.1, the traditional RTA model works properly only in a small horizontal angle misalignment situation. Therefore, it is necessary to modify the attitude representation, improve the alignment accuracy, and enhance the performance of the initialization of the slave SINS.

Attitude rotation quaternion has superior merits of non-singularity, high precision, and simplicity of calculation. When a vector rotates about a single instantaneous axis at a specific angle, the propagation of the kinematics of rotation quaternion does not have any singularity and assumptions about the rotation angles. Thus, the attitude rotation quaternion outperforms the Euler angle when describing arbitrary angle misalignments. Since the unit quaternion is not closed for subtraction, a multiplicative quaternion error is used to represent the distance from the attitude quaternion of the master reference and guarantee that the quaternion error after operations still lies in unit quaternion sphere. Additionally, the differential equations of quaternion error are derived by the quaternion multiplication of attitude rotation quaternions, that is, we can apply this quaternion parameterization in all possible scenarios.

The attitude rotation quaternion needs to be established at first. The kinematics solution for the attitude rotation quaternion defines the desired rotational motion for marine vessels. The quaternion error in [27] is defined as

$$\delta q = q^{-1} \otimes \hat{q}, \quad (2)$$

where $\hat{q}$ represents the reference attitude rotation quaternion, q^{-1} is the inverse of the measurement attitude rotation quaternion, $\otimes$ is a quaternion product, and δq is a unit-vector quaternion error.

Because we initialize the slave SINS with the no-error navigation information from the master system, the master body-to-grid frame rotation quaternion q_m^G can substitute the reference rotation quaternion $\hat{q}$, where the mater SINS may compute and calibrate q_m^G thoroughly via the master navigation computer. Meanwhile, the measurement rotation quaternion q can be expressed as the computed slave body-to-grid frame rotation quaternion $q_{s'}^G$, which implies the physical attitude misalignments. Thus, a unit quaternion error δq is treated as the measurement misalignment quaternion $q_m^{s'}$ between the two available (i.e., slave and master) frames. (2) can be rewritten and then taken its time derivative as

$$\dot{q}_m^{s'} = \frac{d\left(q_{s'}^G\right)^{-1}}{dt} \otimes q_m^G + \left(q_{s'}^G\right)^{-1} \otimes \frac{dq_m^G}{dt}. \quad (3)$$

The kinematics of quaternion evolve in time according to the differential equation.

$$\dot{q}_m^G = \frac{1}{2} q_m^G \otimes \omega_{Gm}^m \quad (4)$$

A unit-vector rotation quaternion times its inverse equals identity, that is, $q_{s'}^G \otimes \left(q_{s'}^G\right)^{-1} = [\,1\ 0\ 0\ 0\,]^T$.Then, the derivative of the identity is performed as $\dot{q}_{s'}^G \otimes q_{s'}^{G^{-1}} + q_{s'}^G \otimes \dot{q}_{s'}^{G^{-1}} = 0$.

After rearrangement, the derivative of the inverse quaternion evolves as:

$$\dot{q}_{s'}^{G^{-1}} = \frac{1}{2}\hat{\omega}_{Gs}^{s} \otimes q_{s'}^{G^{-1}}. \tag{5}$$

Substituting (23) and (5) into (3) yields

$$\begin{aligned}\dot{q}_m^{s'} &= \frac{1}{2}(q_G^{s'} \otimes \hat{\omega}_{sG}^{G} \otimes q_m^G + q_G^{s'} \otimes q_m^G \otimes \omega_{Gm}^m) \\ &= \frac{1}{2}(q_m^{s'} \otimes \omega_{Gm}^m - \hat{\omega}_{Gs}^{s} \otimes q_m^{s'})\end{aligned} \tag{6}$$

where ω_{Gm}^m is the rotation rate of m-frame relative to G-frame, $\hat{\omega}_{Gs}^s$ is the slave estimate of the body-from-grid frame rotation rate, but $\hat{\omega}_{Gs}^s$ contains errors of the slave system. Because the algorithm executes computations in the slave system, the data will be extracted from the slave SINS for update evolutions. Thus, introducing the actual misalignment quaternion q_m^s as a system state, the rotation rate ω_{Gm}^m can be rewritten by $\hat{\omega}_{Gs}^s$ as:

$$\omega_{Gm}^m = (q_m^s)^{-1} \otimes (\hat{\omega}_{Gs}^s - \varepsilon) \otimes q_m^s. \tag{7}$$

Substituting (6) into (5), the quaternion-based attitude error equations for the polar RTA in the grid frame are:

$$\begin{aligned}\dot{q}_m^{s'} &= \frac{1}{2}q_m^{s'} \otimes (q_m^s)^{-1} \otimes \hat{\omega}_{Gs}^s \otimes q_m^s - \frac{1}{2}\hat{\omega}_{Gs}^s \otimes q_m^{s'} \\ &\quad - \frac{1}{2}q_m^{s'} \otimes (q_m^s)^{-1} \otimes \varepsilon \otimes q_m^s \\ \dot{q}_m^s &= 0.\end{aligned} \tag{8}$$

B. VELOCITY ERROR EQUATION

Due to the different placement between the master and slave SINS, the lever arm commonly occurs in the RTA and causes the slave system to figure out an extra velocity, known as the lever-arm effect. The lever-arm velocity is represented as

$$\boldsymbol{V}_r^G = \boldsymbol{q}_m^G \otimes (\boldsymbol{\omega}_{im}^m \times \boldsymbol{r}^m) \otimes \left(\boldsymbol{q}_m^G\right)^{-1} \tag{9}$$

where $\boldsymbol{\omega}_{im}^m$ is the master body-from-inertial frame rotation rate in the master body frame, and $\boldsymbol{r}^m$ is a dynamic lever-arm length.

And the time derivative of lever-arm velocity is

$$\begin{aligned}\dot{\boldsymbol{V}}_r^G &= \frac{\mathrm{d}}{\mathrm{dt}}\left\{\boldsymbol{q}_i^G \otimes \boldsymbol{q}_m^i \otimes (\boldsymbol{\omega}_{im}^m \times \boldsymbol{r}^m) \otimes \left(\boldsymbol{q}_m^i\right)^{-1} \otimes \left(\boldsymbol{q}_i^G\right)^{-1}\right\} \\ &= \boldsymbol{q}_m^G \otimes (\dot{\boldsymbol{\omega}}_{im}^m \times \boldsymbol{r}^m + \boldsymbol{\omega}_{im}^m \times \dot{\boldsymbol{r}}^m) \otimes \left(\boldsymbol{q}_m^G\right)^{-1} \\ &\quad - \boldsymbol{\omega}_{iG}^G \times \boldsymbol{q}_m^G \otimes (\boldsymbol{\omega}_{im}^m \times \boldsymbol{r}^m) \otimes \left(\boldsymbol{q}_m^G\right)^{-1} \\ &= \boldsymbol{q}_m^G \otimes \boldsymbol{a}_r^m \otimes \left(\boldsymbol{q}_m^G\right)^{-1} - \boldsymbol{\omega}_{iG}^G \times \boldsymbol{V}_r^G\end{aligned} \tag{10}$$

where $\boldsymbol{a}_r^m$ is the acceleration of the lever arm in the m-frame, and $\boldsymbol{\omega}_{iG}^G$ is the rotation rate of the grid navigation frame relative to the inertial frame projected in the G-frame.

The deck easily deforms in sea-beaten situations, and its high-frequency deformation angles may be modeled as a second-order Markov process. Then, the dynamic lever arm couples with deformation angels and these elements are thereby expanded into the traditional states of the filter [26]. Nevertheless, its accuracy of alignment is at the cost of computation amounts and aligning time. In comparison, we can add and magnify the process noise, instead of modeling into the lever-arm equation, to compensate for the removal of associated flexural deformation terms [27]. Thus, the differential equation for the dynamic lever arm is rewritten as:

$$\dot{r}_m = w_r \tag{11}$$

where w_r is the process noise of lever arm, modeled as the white noise.

In the traditional rapid transfer alignment model, attitude angle misalignments couple with the velocity via the cosine direction matrix of Euler angles. Thus, the velocity model of quaternion-based RTA should be rewritten.

Amid rapid transfer alignment, the master SINS is regarded as a non-error system. Thus, according to [10], the differential equation of velocity is derived as

$$\dot{V}_m^G = q_m^G \otimes f_m^m \otimes \left(q_m^G\right)^{-1} - (2\omega_{ie}^G + \omega_{eG}^G) \times V_m^G + g_m^G, \tag{12}$$

where V_m^G, q_m^G, f_m^m, and g_m^G are the velocity, attitude rotation quaternion, special force, and gravity vector of the master SINS. The ω_{ie}^G is the rotational angular velocity of the earth projected in the grid navigation frame, and ω_{eG}^G is the angular rate of the grid frame relative to the earth frame projected in the grid frame, which can be expressed below.

$$\begin{aligned}\omega_{ie}^G &= \mathrm{C}_n^G \omega_{ie}^n \\ &= \begin{bmatrix} -\omega_{ie}\cos\varphi\sin\sigma \\ \omega_{ie}\cos\varphi\cos\sigma \\ \omega_{ie}\sin\varphi \end{bmatrix}\end{aligned}$$

where φ is the geographic latitude; σ is the angle between true north and grid north axis.

$$\omega_{eG}^G = \begin{bmatrix} \omega_{eGx}^G \\ \omega_{eGy}^G \\ \omega_{eGz}^G \end{bmatrix} = \begin{bmatrix} \frac{1}{\tau_f} & -\frac{1}{R_y} \\ \frac{1}{R_x} & -\frac{1}{\tau_f} \\ \frac{\kappa}{\tau_f} & -\frac{\kappa}{R_y} \end{bmatrix} \begin{bmatrix} v_E^G \\ v_N^G \end{bmatrix}$$

where v_E^G and v_N^G are the east and north velocity in the grid navigation frame. Other parameters are as follows:

$$\begin{cases} \frac{1}{R_x} = \frac{\sin^2\sigma}{R_{Mh}} + \frac{\cos^2\sigma}{R_{Nh}} \\ \frac{1}{R_y} = \frac{\cos^2\sigma}{R_{Mh}} + \frac{\sin^2\sigma}{R_{Nh}} \\ \frac{1}{\tau_f} = \left(\frac{1}{R_{Mh}} - \frac{1}{R_{Nh}}\right)\sin\sigma\cos\sigma \\ \kappa = \frac{\sin\lambda\cos\varphi}{\sqrt{1-\cos^2\varphi\sin^2\lambda}} \end{cases}$$

where λ is the geographic longitude, and R_{Nh} is the earth prime radius.

The slave velocity evolves in time according to the following differential equation because of the gyros drift and accelerometers bias in practice.

$$\dot{V}_{s'}^{G} = q_{s'}^{G} \otimes \hat{f}_{s}^{s} \otimes \left(q_{s'}^{G}\right)^{-1} - (2\hat{\omega}_{ie}^{G} + \hat{\omega}_{eG}^{G}) \times V_{s'}^{G} + \hat{g}_{s}^{G}, \tag{13}$$

where $V_{s'}^{G}$ is the slave velocity solution computed in G-frame, and $q_{s'}^{G}$ is the computed slave attitude rotation quaternion; $\hat{f}_{s}^{s}$ is the measured slave accelerometers in slave body frame; $\hat{\omega}_{ie}^{G}$, $\hat{\omega}_{eG}^{G}$, and $\hat{g}_{s}^{G}$ are slave estimate navigation parameters

Because the master reference system initializes the slave SINS, the relationship between the master true and slave measured special force is

$$\begin{aligned}\hat{f}_{s}^{s} &= f_{s}^{s} + \nabla^{s} \\ &= q_{m}^{s} \otimes f_{s}^{m} \otimes \left(q_{m}^{s}\right)^{-1} + \nabla^{s} \\ &= q_{m}^{s} \otimes \left(f_{m}^{m} + a_{r}^{m}\right) \otimes \left(q_{m}^{s}\right)^{-1} + \nabla^{s},\end{aligned} \tag{14}$$

where ∇^{s} is the drift of the slave accelerometer.

It will be assumed that the gravitational compensation for the master and slave system is identical so that the master and slave gravitational effects cancel perfectly. Subtracting (13) from (12) yields

$$\begin{aligned}\dot{V}_{s'}^{G} - \dot{V}_{m}^{G} &= q_{s'}^{G} \otimes \hat{f}_{s}^{s} \otimes q_{G}^{s'} - q_{s'}^{G} \otimes q_{m}^{s'} \otimes f_{m}^{m} \otimes q_{s'}^{m} \otimes q_{G}^{s'} \\ &\quad - \left(2\omega_{ie}^{G} + \omega_{eG}^{G}\right) \times \left(V_{s'}^{G} - V_{m}^{G}\right) \\ &= q_{s'}^{G} \otimes \left(\hat{f}_{s}^{s} - q_{m}^{s'} \otimes f_{m}^{m} \otimes q_{s'}^{m}\right) \otimes q_{G}^{s'} \\ &\quad - \left(2\omega_{ie}^{G} + \omega_{eG}^{G}\right) \times \left(V_{s'}^{G} - V_{m}^{G}\right) \\ &= q_{s'}^{G} \otimes \left(\hat{f}_{s}^{s} - q_{m}^{s'} \otimes q_{s}^{m} \otimes \hat{f}_{s}^{s} \otimes q_{m}^{s} \otimes q_{s'}^{m}\right) \otimes q_{G}^{s'} \\ &\quad + a_{r}^{G} - \left(2\omega_{ie}^{G} + \omega_{eG}^{G}\right) \times \left(V_{s'}^{G} - V_{m}^{G}\right) \\ &\quad - \left(2\delta\omega_{ie}^{G} + \delta\omega_{eG}^{G}\right) \times V_{s}^{G} + q_{s}^{G} \otimes \nabla^{s} \otimes q_{G}^{s}\end{aligned} \tag{15}$$

The velocity error is defined with the lever-arm effect as

$$\delta V^{G} = V_{s'}^{G} - V_{m}^{G} - V_{r}^{G}. \tag{16}$$

Substituting (10) and (16) into (15) generates

$$\begin{aligned}\delta\dot{V}^{G} &= q_{s'}^{G} \otimes \left(\hat{f}_{s}^{s} - q_{m}^{s'} \otimes q_{s}^{m} \otimes \hat{f}_{s}^{s} \otimes q_{m}^{s} \otimes q_{s'}^{m}\right) \otimes q_{G}^{s'} + q_{s}^{G} \\ &\quad \otimes \nabla^{s} \otimes q_{G}^{s} - \left(2\omega_{ie}^{G} + \omega_{eG}^{G}\right) \times \left(V_{s'}^{G} - V_{m}^{G}\right) \\ &\quad - \left(2\delta\omega_{ie}^{G} + \delta\omega_{eG}^{G}\right) \times V_{s}^{G} + a_{r}^{G} - \dot{V}_{r}^{G} \\ &= q_{s'}^{G} \otimes \left(\hat{f}_{s}^{s} - q_{m}^{s'} \otimes q_{s}^{m} \otimes \hat{f}_{s}^{s} \otimes q_{m}^{s} \otimes q_{s'}^{m}\right) \otimes q_{G}^{s'} + q_{s}^{G} \\ &\quad \otimes \nabla^{s} \otimes q_{G}^{s} - \left(2\omega_{ie}^{G} + \omega_{eG}^{G}\right) \times \left(V_{s'}^{G} - V_{m}^{G} - V_{r}^{G}\right) \\ &\quad - \left(2\delta\omega_{ie}^{G} + \delta\omega_{eG}^{G}\right) \times V_{s}^{G} - \left(2\omega_{ie}^{G} + \omega_{eG}^{G}\right) \\ &\quad \times \boldsymbol{V}_{r}^{G} + \boldsymbol{\omega}_{iG}^{G} \times \boldsymbol{V}_{r}^{G} \\ &= q_{s'}^{G} \otimes \left(\hat{f}_{s}^{s} - q_{m}^{s'} \otimes q_{s}^{m} \otimes \hat{f}_{s}^{s} \otimes q_{m}^{s} \otimes q_{s'}^{m}\right) \otimes q_{G}^{s'} + q_{s}^{G} \\ &\quad \otimes \nabla^{s} \otimes q_{G}^{s} - \left(2\omega_{ie}^{G} + \omega_{eG}^{G}\right) \times \delta V^{G} \\ &\quad - \left(2\delta\omega_{ie}^{G} + \delta\omega_{eG}^{G}\right) \times V_{s}^{G} - \omega_{ie}^{G} \\ &\quad \times \left(\boldsymbol{q}_{m}^{G} \otimes \left(\boldsymbol{\omega}_{im}^{m} \times \boldsymbol{r}^{m}\right) \otimes \boldsymbol{q}_{G}^{m}\right)\end{aligned} \tag{17}$$

Due to data extracted from the slave SINS, (17) can be rewritten as

$$\begin{aligned}\delta\dot{V}^{G} &= q_{s'}^{G} \otimes \left(\hat{f}_{s}^{s} - q_{m}^{s'} \otimes q_{s}^{m} \otimes \hat{f}_{s}^{s} \otimes q_{m}^{s} \otimes q_{s'}^{m}\right) \otimes q_{G}^{s'} + q_{s}^{G} \\ &\quad \otimes \nabla^{s} \otimes q_{G}^{s} - \left(2\omega_{ie}^{G} + \omega_{eG}^{G}\right) \times \delta V^{G} - \left(2\delta\omega_{ie}^{G}\right. \\ &\quad \left. + \delta\omega_{eG}^{G}\right) \times V_{s}^{G} - \omega_{ie}^{G} \times \left(\boldsymbol{q}_{s'}^{G} \otimes q_{m}^{s'} \otimes \left(\left(q_{s}^{m}\right.\right.\right. \\ &\quad \left.\left.\left. \otimes \left(\hat{\boldsymbol{\omega}}_{is}^{s} - \varepsilon\right) \otimes q_{m}^{s}\right) \times \boldsymbol{r}^{m}\right) \otimes q_{s'}^{m} \otimes \boldsymbol{q}_{G}^{s'}\right)\end{aligned} \tag{18}$$

The measurement errors $\delta\omega_{ie}^{G}$ and $\delta\omega_{eG}^{G}$ can be derived as

$$\delta\omega_{ie}^{G} = \omega_{ie} \begin{bmatrix} \cos\varphi \sin\sigma \\ \cos\varphi \cos\sigma \\ 0 \end{bmatrix} \delta\sigma + \begin{bmatrix} \sin\varphi \sin\sigma \\ \sin\varphi \cos\sigma \\ \cos\varphi \end{bmatrix} \delta\varphi \tag{19}$$

$$\begin{aligned}\delta\omega_{eG}^{G} &= \begin{bmatrix} 0 & 0 & \dfrac{v_{GN}}{(R_{\mathrm{e}})^{2}} \\ 0 & 0 & -\dfrac{v_{GE}}{(R_{\mathrm{e}})^{2}} \\ \dfrac{v_{GN}\sin\sigma}{R_{e}\sin^{2}L} & 0 & \dfrac{v_{GN}\cot\varphi\sin\sigma}{(R_{\mathrm{e}})^{2}} \end{bmatrix} \begin{bmatrix} \delta\varphi \\ \delta\lambda \\ \delta h \end{bmatrix} \\ &\quad + \begin{bmatrix} 0 & -\dfrac{1}{R_{\mathrm{e}}} & 0 \\ \dfrac{1}{R_{\mathrm{e}}} & 1 & 0 \\ 0 & -\dfrac{\cot\varphi\sin\sigma}{R_{e}} & 0 \end{bmatrix} \begin{bmatrix} \delta v_{GE} \\ \delta v_{GN} \\ \delta v_{GU} \end{bmatrix} \\ &\quad + \begin{bmatrix} 0 \\ 0 \\ \dfrac{v_{GN}\cot\varphi\cos\sigma}{(R_{e})^{2}} \end{bmatrix} \delta\sigma\end{aligned} \tag{20}$$

$$\delta\sigma = \frac{\sin\lambda}{1 - \cos^{2}\varphi\sin^{2}\lambda}\delta\lambda + \frac{\sin\lambda\cos\lambda\cos\varphi}{1 - \cos^{2}\varphi\sin^{2}\lambda}\delta\varphi. \tag{21}$$

From (19) to (21), the error of $2\delta\omega_{ie}^{G} + \delta\omega_{eG}^{G}$ is primarily induced by the position error between two SINS systems [26]. However, this error can be neglected since the distance between the two systems is extremely short relative to the radii of the earth, and RTA time is rather short. Additionally, (38) can be simplified without the lever-arm effect and position errors as

$$\begin{aligned}\delta\dot{V}^{G} &= q_{s'}^{G} \otimes \left(\hat{f}_{s}^{s} - q_{m}^{s'} \otimes q_{s}^{m} \otimes \hat{f}_{s}^{s} \otimes q_{m}^{s} \otimes q_{s'}^{m}\right) \otimes q_{G}^{s'} \\ &\quad - \left(2\omega_{ie}^{G} + \omega_{eG}^{G}\right) \times \delta V^{G} + q_{s}^{G} \otimes \nabla^{s} \otimes q_{G}^{s}.\end{aligned} \tag{22}$$

III. FILTER MODEL

According to the error equations derived in section II, the filter models for the proposed polar RTA, including the dynamic and observation models, can be presented in this section.

A. DYNAMIC MODEL

Firstly, the slave gyros and accelerometers can be modeled as:

$$\begin{aligned} \nabla^b &= \nabla_c^b + \nabla_w^b \\ \varepsilon^b &= \varepsilon_c^b + \varepsilon_w^b \end{aligned} \tag{23}$$

where ∇_c^b and ε_c^b are constant errors; ∇_w^b and ε_w^b are random errors.

Then, the states should be determined. We consider the disturbance and choose the attitude rotation quaternion error $q_m^{s'}$, the actual attitude rotation quaternion error q_m^s, the grid velocity error δV^G, the constant drift of gyro ∇_c^b, the constant bias of accelerometer ε_c^b,and the dynamic lever-arm length $\boldsymbol{r}^m$ as the system states. Thus, the states are listed as follows:

$$X_1 = \left[(q_m^{s'})^T \quad (q_m^s)^T \quad (\delta v^G)^T \quad (\nabla_s^s)^T \quad (\varepsilon_s^s)^T \quad (r_m)^T \right]_{18\times 1}^T.$$

Combining the (8), (11), (18), and (23), the dynamic error equations can be presented as follows:

$$\begin{cases} \dot{\boldsymbol{q}}_m^{s'} = \frac{1}{2}\left(\boldsymbol{q}_m^{s'} \otimes \left(\boldsymbol{q}_m^s\right)^{-1} \otimes \hat{\omega}_{Gs}^s \otimes \boldsymbol{q}_m^s - \hat{\omega}_{Gs}^s \otimes \boldsymbol{q}_m^{s'} \right. \\ \quad \left. - \boldsymbol{q}_m^{s'} \otimes \left(\boldsymbol{q}_m^s\right)^{-1} \otimes \varepsilon \otimes \boldsymbol{q}_m^s\right) \\ \dot{\boldsymbol{q}}_m^s = 0 \\ \delta\dot{V} = \boldsymbol{q}_{s'}^G \otimes \left(\hat{f}_s^s - \boldsymbol{q}_m^{s'} \otimes \boldsymbol{q}_s^m \otimes \hat{f}_s^s \otimes \boldsymbol{q}_m^s \otimes \boldsymbol{q}_{s'}^m \otimes \boldsymbol{q}_G^{s'}\right. \\ \quad + \boldsymbol{q}_s^G \otimes \nabla^s \otimes \boldsymbol{q}_G^s - \left(2\omega_{ie}^G + \omega_{eG}^G\right) \times \delta V^G \\ \quad - \left(2\delta\omega_{ie}^G + \delta\omega_{eG}^G\right) \times V_s^G \\ \quad - \omega_{ie}^G \times \left(\boldsymbol{q}_{s'}^G \otimes \boldsymbol{q}_m^{s'} \otimes \left(\left(\boldsymbol{q}_s^m \otimes \left(\hat{\boldsymbol{\omega}}_{is}^s - \varepsilon\right)\right.\right.\right. \\ \quad \left.\left.\left. \otimes\ \boldsymbol{q}_m^s\right) \times \boldsymbol{r}^m\right) \otimes \boldsymbol{q}_{s'}^m \otimes \boldsymbol{q}_G^{s'}\right) \\ \dot{\nabla}_s^s = 0 \\ \dot{\varepsilon}_s^s = 0 \\ \dot{\boldsymbol{r}}_m = \boldsymbol{w}_r \end{cases} \tag{24}$$

The above dynamic model is defined as Algorithm 1. For the simplicity and speed of the polar RTA, we can remove the lever-arm length from the systematic states and its associated terms from the dynamic model, which is defined as Algorithm 2. The system states are rewritten as:

$$X_2 = \left[(q_m^{s'})^T \quad (q_m^s)^T \quad (\delta v^G)^T \quad (\nabla_s^s)^T \quad (\varepsilon_s^s)^T \right]_{15\times 1}^T$$

The differential equations combine the (9), (11), (22), and (23). The dynamic model for Algorithm 2 can be rearranged as follows:

$$\begin{cases} \dot{q}_m^{s'} = \frac{1}{2}\left(q_m^{s'} \otimes \left(q_m^s\right)^{-1} \otimes \hat{\omega}_{Gs}^s \otimes q_m^s - \hat{\omega}_{Gs}^s \otimes q_m^{s'} \right. \\ \quad \left. - q_m^s \otimes \left(q_m^s\right)^{-1} \otimes \varepsilon \otimes q_m^s\right) \\ \dot{q}_m^s = 0 \\ \delta\dot{V} = q_{s'}^G \otimes \left(\hat{f}_s^s - q_m^{s'} \otimes q_s^m \otimes \hat{f}_s^s \otimes q_m^s \otimes q_{s'}^m\right) \otimes q_G^{s'} \\ \quad - \left(2\omega_{ie}^G + \omega_{eG}^G\right) \times \delta V^G + q_s^G \otimes \nabla^s \otimes q_G^s \\ \dot{\nabla}_s^s = 0 \\ \dot{\varepsilon}_s^s = 0 \end{cases} \tag{25}$$

B. MEASUREMENT MODEL

In the case of a large azimuth misalignment in the traditional polar RTA, the attitude observation can be extracted from

Therefore, the measurement equation for attitude can be expressed as

$$Z_{atti} = \begin{bmatrix} C_m^{s'}(2,3) \\ C_m^{s'}(1,3) \\ C_m^{s'}(1,2) \end{bmatrix} = \begin{bmatrix} \phi_{mx}^G \\ -\phi_{my}^G \\ \sin\phi_{mz}^G \end{bmatrix} + v \tag{27}$$

The component along the z-axis in the measurement equation comprises a sine function of a large azimuth misalignment, which cannot be linearized by reason of accuracy. If the horizontal angle misalignment is large enough, we may not linearize the sine function of the measurement misalignment to the angle itself, which is prone to introduce an error in estimation.

The strapdown inertial navigation system computes and outputs attitude rotation quaternions in practice, and the star sensor on marine vessels is capable of opting quaternions as an attitude output. Thus, it is possible to adopt the attitude rotation quaternions as an observation for polar RTA. The difference in velocity and the multiplicative quaternion error via quaternion product are selected as the observations. The observations with the lever-arm compensation for Algorithm 1 are modeled as follows:

$$\begin{aligned} Z_v &= V_{s'}^G - V_m^G = \delta V^G + q_m^G \otimes (\omega_{im}^m \times r^m) \otimes q_G^m \\ Z_q &= q_m^{s'} = \left(q_{s'}^G\right)^{-1} \otimes q_m^G, \end{aligned} \tag{28}$$

The observation model is expressed in the forms of a matrix as:

$$Z = Hx + v \tag{29}$$

where the observation matrix H is specified for Algorithm 1 as $H = \begin{bmatrix} I_{2\times 2} & 0_{2\times 4} & 0_{2\times 9} & \left(C(q_m^G)\omega_{im}^m\times\right)_{2\times 3} \\ 0_{4\times 2} & I_{4\times 4} & 0_{4\times 9} & 0_{4\times 3} \end{bmatrix}$, $C(q_m^G)$ is the cosine direction matrix transformed from the attitude rotation quaternion q_m^G, and the measurement noise v is the zero-mean Gaussian white noise with covariance matrix R.

In contrast, the observations for Algorithm 2 are simplified as following equations.

$$\begin{aligned} Z_v &= V_{s'}^G - V_m^G = \delta V^G \\ Z_q &= q_m^{s'} = \left(q_{s'}^G\right)^{-1} \otimes q_m^G \end{aligned} \tag{30}$$

The observation matrix H for (30) is specified as $H = \begin{bmatrix} I_{2\times 2} & 0_{2\times 4} & 0_{2\times 9} \\ 0_{4\times 2} & I_{4\times 4} & 0_{4\times 9} \end{bmatrix}$. Compared with the traditional measurement models, the option of the velocity and quaternion observation linearizes the measurement models, which renders the z-axis attitude measurement free from a sine function as well.

Furthermore, the observations require to be divided into two segments, the non-quaternion and quaternion vector, since the measurement noise of quaternion is coupled via

quaternion multiplication rather than addition in Euclidean space. Thus, (29) is rewritten as follows:

$$\begin{aligned} Z_v &= \delta V^G + v_v \\ Z_q &= q_m^{s'} \otimes v_q \end{aligned} \tag{31}$$

where v_v is the measurement noise of the non-quaternion states, and v_q is the measurement noise of the quaternion components.

C. THE APPLICATION OF THE AUGMENTED UNSCENTED KALMAN FILTER

As known, the extended Kalman filter (EKF) is a widely used approach for a non-linear filter algorithm. Exploiting the assumption that all transformations are quasi-linear, the EKF simply linearizes all non-linear transformations and substitutes Jacobian matrices for the linear transformations in the KF equations. However, it is complicated to enforce Jacobians to expand models, since the estimated state quantity in the proposed model is at least 15. Due to the application of local linearization at a single point in the state space, the high nonlinearity of models must induce extra linearized errors.

A prevailing alternative estimator is UKF. According to the (24) (25) and (31), the quaternion noise is coupled via quaternion product with states. Hence, the augmented UKF is employed and adjusted here to surmount the non-additive noise, which expands the process and measurement noises into system states and adds these noise covariances into the initial state error covariance matrix.

According to the (24) (25) and (31), the nonlinear discrete filter model is expressed as:

$$\begin{cases} \boldsymbol{X}_k = f\left(\boldsymbol{X}_{k-1}, w_k\right) \\ \boldsymbol{Z}_k = h\left(\boldsymbol{X}_k, v_k\right), \end{cases} \tag{32}$$

where w_k (m-dimension) and v_k(l-dimension) represent the process and measurement noise at time k, respectively. The primary details of the augmented UKF are explained as follows.

(1) State Augmented

$$\begin{aligned} \bar{\boldsymbol{X}}_{k-1}^a &= [\left(\boldsymbol{X}_{k-1}^{(1or2)}\right)^T \quad w_{k-1}^T \quad v_{k-1}^T]^T \\ \bar{\boldsymbol{P}}_{k-1}^a &= \begin{bmatrix} \boldsymbol{P}_{k-1} & 0 & 0 \\ 0 & \boldsymbol{Q}_{k-1} & 0 \\ 0 & 0 & \boldsymbol{R}_{k-1} \end{bmatrix} \end{aligned} \tag{33}$$

The augmented state vector $\bar{\boldsymbol{X}}_{k-1}^a$ and augmented covariance matrix $\bar{\boldsymbol{P}}_{k-1}^a$ at time k − 1 are presented as (33), in which $X_{k-1}^{(1or2)}$ is system states in Algorithm 1 or Algorithm 2. $\bar{\boldsymbol{P}}_{k-1}^a$, $\boldsymbol{Q}_{k-1}$ and $\boldsymbol{R}_{k-1}$ are the state error variance matrix, system process noise covariance matrix, and measurement noise covariance matrix at time k − 1.

(2) Initialization

The process and measurement noise are zero-mean Gaussian white noise. Thus, the augmented states initialize as follows.

$$\bar{\boldsymbol{X}}_0^a = [\,\boldsymbol{X}_{(1or2),0}^T \quad 0^T \quad 0^T\,]^T \quad \bar{\boldsymbol{P}}_0^a = \begin{bmatrix} \boldsymbol{P}_0 & 0 & 0 \\ 0 & \boldsymbol{Q}_0 & 0 \\ 0 & 0 & \boldsymbol{R}_0 \end{bmatrix} \tag{34}$$

We generate sigma points $\boldsymbol{\chi}_{k-1}^a$ as following rules.

$$\begin{cases} \boldsymbol{\chi}_{k-1}^a(0) = \bar{\boldsymbol{X}}_{k-1}^a \\ \boldsymbol{\chi}_{i,k-1}^a = \bar{\boldsymbol{X}}_{k-1}^a + \left(\sqrt{(L+\lambda)\,\bar{\boldsymbol{P}}_{k-1}^a}\right)_i, \\ \qquad i = 1, 2, \ldots, L \\ \boldsymbol{\chi}_{i,k-1}^a = \bar{\boldsymbol{X}}_{k-1}^a - \left(\sqrt{(L+\lambda)\,\bar{\boldsymbol{P}}_{k-1}^a}\right)_i, \\ \qquad i = n+1, \ldots, 2L, \end{cases} \tag{35}$$

where $L = n + m + l$, and n represents the quantity of the system states.

The associated weights are

$$\begin{aligned} W_0^m &= \lambda/\left(n+\lambda\right) W_0^c = \lambda/\left(n+\lambda\right) + \left(1 - \alpha^2 + \beta\right) \\ W_i^m &= W_i^c = 0.5/\left(n+\lambda\right), \quad i = 1, 2, \ldots, 2L \\ \lambda &= \alpha^2(n+\kappa) - n, \end{aligned} \tag{36}$$

where α implies the sigma-point distribution, and it usually selects a small value; κ is a scaled factor and normally adopts $3 - n$; β for Gaussian distribution chooses 2.

(3) Time Update

After the nonlinear transformation function $f\left(\boldsymbol{X}_{k-1}, w_k\right)$ in (32), we can obtain the one-step predicted mean and variance of system states, at time k, as:

$$\begin{aligned} \boldsymbol{\chi}_{i,k|k-1}^a &= f\left(\boldsymbol{\chi}_{i,k-1}^a\right), \bar{\boldsymbol{X}}_k^{a^-} = \sum_{i=0}^{2L} W_i^m \boldsymbol{\chi}_{i,k|k-1}^a \\ \bar{\boldsymbol{P}}_k^{a^-} &= \sum_{i=0}^{2L} W_i^c \left[\boldsymbol{\chi}_{i,k|k-1}^a - \bar{\boldsymbol{X}}_k^{a^-}\right]\left[\boldsymbol{\chi}_{i,k|k-1}^a - \bar{\boldsymbol{X}}_k^{a^-}\right]^{\mathrm{T}}. \end{aligned} \tag{37}$$

(4) Measurement Update

Through the measurement equation $h\left(\boldsymbol{X}_k, v_k\right)$ in (32), we obtain the one-step predicted mean of measurements, its

$$\mathrm{C}_m^{s'} = \begin{bmatrix} \cos\phi_{mz}^G & \sin\phi_{mz}^G & -\phi_{my}^G \\ -\sin\phi_{mz}^G & \cos\phi_{mz}^G & \phi_{mx}^G \\ \phi_{my}^G\cos\phi_{mz}^G + \phi_{mx}^G\sin\phi_{mz}^G & \phi_{my}^G\sin\phi_{mz}^G - \phi_{mx}^G\cos\phi_{mz}^G & 1 \end{bmatrix}. \tag{26}$$

variance and covariance and updates as follows.

$$\begin{aligned}
\boldsymbol{Z}_{i,k|k-1} &= h\left(\boldsymbol{\chi}^{a}_{i,k-1}\right), \hat{\boldsymbol{Z}}^{-}_{k} = \sum_{i=0}^{2L} W^{m}_{i} \boldsymbol{Z}_{i,k|k-1} \\
\bar{\boldsymbol{P}}^{a}_{z_k,z_k} &= \sum_{i=0}^{2L} W^{c}_{i} \left[\boldsymbol{Z}_{i,k|k-1} - \hat{\boldsymbol{Z}}^{-}_{k}\right]\left[\boldsymbol{Z}_{i,k|k-1} - \hat{\boldsymbol{Z}}^{-}_{k}\right]^{\mathrm{T}} \\
\bar{\boldsymbol{P}}^{a}_{x^{a}_{k},z_k} &= \sum_{i=0}^{2L} W^{c}_{i} \left[\boldsymbol{\chi}^{a}_{i,k|k-1} - \bar{\boldsymbol{X}}^{a-}_{k}\right]\left[\boldsymbol{Z}_{i,k|k-1} - \hat{\boldsymbol{Z}}^{-}_{k}\right]^{\mathrm{T}} \\
\boldsymbol{K}_{k} &= \bar{\boldsymbol{P}}^{a}_{x^{a}_{k},z_k} \cdot \left(\bar{\boldsymbol{P}}^{a}_{z_k,z_k}\right)^{-1}, \bar{\boldsymbol{P}}^{a}_{k} = \bar{\boldsymbol{P}}^{a-}_{k} - \boldsymbol{K}_{k} \cdot \bar{\boldsymbol{P}}^{a}_{z_k,z_k} \cdot \boldsymbol{K}^{\mathrm{T}}_{k} \\
\bar{\boldsymbol{X}}^{a}_{k} &= \bar{\boldsymbol{X}}^{a-}_{k} + \boldsymbol{K}_{k}\left(\boldsymbol{Z}_{k} - \hat{\boldsymbol{Z}}^{-}_{k}\right) \qquad (38)
\end{aligned}$$

(5) Normalization Maintenance

After each step, we must enforce the (39) on the actual and measurement misalignment quaternions in augmented state vectors to guarantee the normalization and wait for the next update cycle.

$$\bar{X}^{a}_{q^{s'}_{m}} = \frac{\bar{X}^{a}_{q^{s'}_{m}}}{\left\|\bar{X}^{a}_{q^{s'}_{m}}\right\|}, \bar{X}^{a}_{q^{s}_{m}} = \frac{\bar{X}^{a}_{q^{s}_{m}}}{\left\|\bar{X}^{a}_{q^{s}_{m}}\right\|} \qquad (39)$$

Based on this filtering process, repeating the above steps, continuous estimates can be realized.

IV. RESULTS AND ANALYSIS

An innovative polar RTA using the quaternion matching and the augmented unscented Kalman filter is proposed for 3-axis large attitude misalignments in this article, and the simulations and experiments should be firstly conducted to test its performance. The physical experiment is then performed. However, the experiment is constrained by the geographical location of the author's country to obtain the polar INS data hardly. So, we can carry out the semi-physical simulation, extract the inertial measurement unit (IMU) noise at medium latitudes, and construct the actual data of polar regions.

A. SIMULATION CONDITIONS

Various conditions and maneuvers must be considered to conduct simulations in verisimilar state of the ocean, involving the moderate sea state and maneuvers of the static, uniformly linear, and uniformly accelerated motion.

(1) In the trajectory generator, the swaying motions of the marine vessel are modeled as sine functions, and the parameters are set as: the amplitude/period of attitude in the medium state of polar regions is respectively $10°/3s$, $9°/5s$,and $7°/7s$; the initial phase and heading are 0° and 0°.

(2) Maneuvers of the marine vessels are pre-determined as follows: the latitude and longitude are $89°N$ and $126.67°E$; the uniformly linear velocity is $10nmile/h$; the constant acceleration is $0.1m/s^2$.

(3) The constant drifts of the 3-axis gyros are set to $0.01°/h$, while random errors are the zero-mean Gaussian white noise. The constant biases of the 3-axis accelerometers are $100\mu g$, while random errors are the zero-mean Gaussian white noise.

(4) In the case of 3-axis large angle misalignments, the true ones are reset to 15°, 15°, and 60°; the 3-axis length of lever arm are $1m-2m-2m$, and $15m-10m-40m$. The time of simulation is 60s, and the frequency of filter is $100Hz$.

(5) In the filter for Algorithm 1, the state error covariance matrix $\boldsymbol{P}_0$, system process noise covariance matrix $\boldsymbol{Q}$, and measurement noise covariance matrix $\boldsymbol{R}$ are set respectively as:

$$\begin{aligned}
\boldsymbol{P}_0 &= \mathrm{diag}\left\{\begin{array}{l}(0.05)^2, (0.05)^2, (0.05)^2, (0.05)^2, \\ (0.05)^2, (0.05)^2, (0.05)^2, (0.05)^2, \\ (0.01m/s)^2, (0.01m/s)^2, \\ \left(0.000978m/s^2\right)^2, \left(0.000978m/s^2\right)^2, \\ \left(4.8481\times10^{-8}rad/s\right)^2, \\ \left(4.8481\times10^{-8}rad/s\right)^2, \\ \left(4.8481\times10^{-8}rad/s\right)^2, \\ (0.1m)^2, (0.1m)^2, (0.1m)^2,\end{array}\right\} \\
\boldsymbol{Q} &= \mathrm{diag}\left\{\begin{array}{l}(0.000978m/s^2)^2, (0.000978m/s^2)^2, \\ (2.42405\times10^{-8}rad/s)^2, \\ (2.42405\times10^{-8}rad/s)^2, \\ (2.42405\times10^{-8}rad/s)^2, \\ (0.001m)^2, (0.001m)^2, (0.001m)^2\end{array}\right\} \\
\boldsymbol{R} &= \mathrm{diag}\left\{\begin{array}{l}(0.11m/s)^2, (0.11m/s)^2, \\ \left(0.06°/\sqrt{h}\right)^2, \left(0.06°/\sqrt{h}\right)^2, \\ \left(0.06°/\sqrt{h}\right)^2, \left(0.06°/\sqrt{h}\right)^2\end{array}\right\};
\end{aligned}$$

(6) In the filter for Algorithm 2, the state error covariance matrix $\boldsymbol{P}_0$, system process noise covariance matrix $\boldsymbol{Q}$, and measurement noise covariance matrix $\boldsymbol{R}$ are set respectively as:

$$\begin{aligned}
\boldsymbol{P}_0 &= \mathrm{diag}\left\{\begin{array}{l}(0.05)^2, (0.05)^2, (0.05)^2, (0.05)^2, \\ (0.05)^2, (0.05)^2, (0.05)^2, (0.05)^2, \\ (0.01m/s)^2, (0.01m/s)^2, \\ \left(0.000978m/s^2\right)^2, \left(0.000978m/s^2\right)^2, \\ \left(4.8481\times10^{-8}rad/s\right)^2, \\ \left(4.8481\times10^{-8}rad/s\right)^2, \\ \left(4.8481\times10^{-8}rad/s\right)^2\end{array}\right\} \\
\boldsymbol{Q} &= \mathrm{diag}\left\{\begin{array}{l}(0.00489m/s^2)^2, (0.00489m/s^2)^2, \\ (2.42405\times10^{-7}rad/s)^2, \\ (2.42405\times10^{-7}rad/s)^2, \\ (2.42405\times10^{-7}rad/s)^2\end{array}\right\} \\
\boldsymbol{R} &= \mathrm{diag}\left\{\begin{array}{l}(0.11m/s)^2, (0.11m/s)^2, \\ \left(0.06°/\sqrt{h}\right)^2, \left(0.06°/\sqrt{h}\right)^2, \\ \left(0.06°/\sqrt{h}\right)^2, \left(0.06°/\sqrt{h}\right)^2\end{array}\right\}.
\end{aligned}$$

B. SIMULATION RESULTS AND DISCUSSIONS

The full-information polar quaternion rapid transfer alignment (QRTA) with lever-arm modelling proposed in this article is defined as Model 1 (i.e., Algorithm 1 in section III).

TABLE 1. RMS errors of RTA in medium sea state with misalignment angles of 15°, 15°, and 60°.

Parameters	Model	The static motion	The uniform linear motion	The uniformly accelerated motion
Pitch /(°)	Model 1	0.0418	0.0564	0.0978
	Model 2	1.1929	1.2535	1.2224
Roll /(°)	Model 1	0.0710	0.0563	0.0315
	Model 2	0.7811	0.7609	0.8271
Yaw /(°)	Model 1	0.1448	0.1983	0.1382
	Model 2	3.2278	3.2191	3.2504

The traditional polar RTA with a large azimuth misalignment [11] is defined as Model 2. The simplified polar QRTA without lever-arm modeling and position-induced errors (i.e., Algorithm 2 in section III) is defined as Model 3.

The comparison between Model 1 and Model 2 aims to verify the feasibility and superiority of the QRTA in polar regions. The comparison between Model 1 and Model 3 is designed to verify the robustness of the QRTA in lever-arm effect. Thus, we separate the simulations into two different segments to make the comparison clarified and highlighted.

1) THE FEASIBILITY AND SUPERIORITY OF THE QRTA

Both model 1 and model 2 employ the nonlinear equations and UKF. However, the difference is that model 1 establishes models without assumptions of misalignments, and the UKF is augmented to match non-additive noise. In contrast, the model 2 constructs differential equations under the premise of small horizontal attitude errors, the measurement equations have a nonlinear sine function, and the general UKF is adopted.

The simulation is conducted with the assumptions of the 3-axis angle misalignments of 15°, 15°, and 60° to validate the feasibility and superiority of QRTA. In the medium sea state, the estimate error $\delta\phi_a$ of the physical misalignment ϕ_a^G is depicted under the static, uniform linear, and uniformly accelerated motion in Fig.2. Its root-mean-square (RMS) error is listed in Table 1.

As the estimate error curves of ϕ_a^G shows in Fig.2, the RMS errors in Table 1 verify that the QRTA outperforms the traditional RTA in 3-axis large-angle misalignments. Obviously, the yaw misalignment of the traditional RTA is significantly larger than that through the QRTA. The results demonstrate that the yaw misalignment in QRTA reduces by 95.03%, which is rendered by no approximation during model derivations and the increasing accuracy of horizontal attitude estimates. Comparing the results of Model 1 with that of Model 2, the roll and pitch misalignments reduce by 93.23% and 94.60% because using the actual

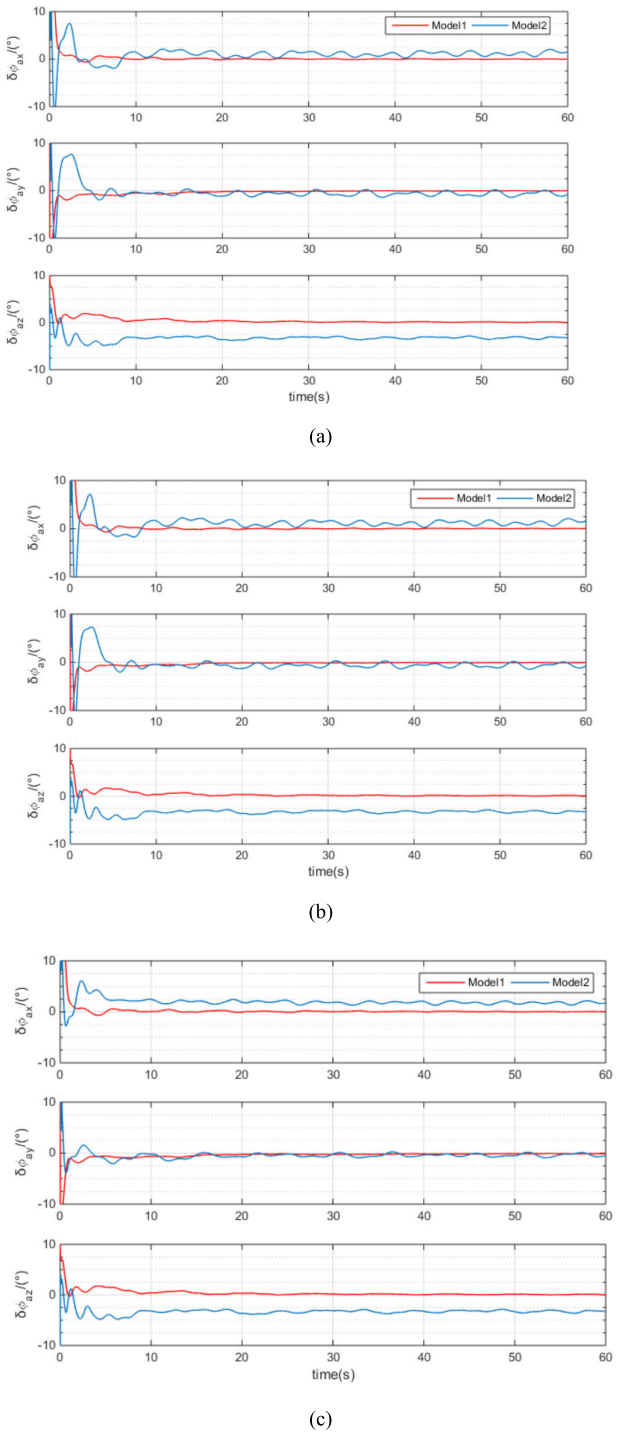

FIGURE 2. Attitude estimate error of ϕ_a^G in the medium sea conditions with misalignment of 15°, 15°, and 60° for various models (a) in the static motion; (b) in the uniform linear motion; (c) in the uniformly accelerated motion.

and measurement misalignment quaternions derive the error models of the pitch and roll misalignments, and we adopt the measurement misalignment quaternion as an observation directly with no approximation assumptions. The traditional RTA with a large azimuth misalignment cannot estimate the

TABLE 2. RMS errors of RTA with various lever-arm length.

Parameters	Model	1m-2m-2m	15m-10m-40m
Pitch /(°)	Model 1	0.0529	0.0494
	Model3	0.0533	0.0514
Roll /(°)	Model 1	0.0305	0.0348
	Model 3	0.0356	0.0379
Yaw /(°)	Model 1	0.1053	0.1801
	Model 3	0.1136	0.1880

attitudes accurately and effectively for large misalignments. Meanwhile, the QRTA shortens alignment time than the traditional RTA in Fig. 2. Thus, the full-information polar QRTA (Algorithm 1 in Section II) based on the augmented UKF can enhance the performance under all possible scenarios of arbitrary misalignments.

2) THE ROBUSTNESS FOR THE LEVER-ARM EFFECT

This section of simulations is solely conducted in the uniform linear motion under moderate sea conditions and various lever-arm lengths. The misalignment is set here as 15°, 15°, and 60°.

With the lever-arm length of 1m, 2m, and 2m, the 3-axis angle misalignment of Model 1 reduces by 0.0004°, 0.0051°, and 0.0083° over that of Model 3. With the lever-arm length of 15m, 10m, and 40m, the 3-axis angle misalignment of Model 1 reduces by 0.002°, 0.0031°, and 0.0079° over that of Model 3. In practice, these errors seldom affect accuracy of RTA. In conclusion, the lever-arm effect barely impacts the performance and accuracy of the QRTA. The reason is that the multiplicative quaternion error takes four components as state variables, and all four components jointly determine the values of the 3-axis angle misalignments. In other words, the proposed algorithm is robust with disturbance of the lever-arm effect.

Meanwhile, in the data processing of simplified QRTA, the operating time of the main program decreases from 67.522s to 45.366s, the measurement equation cuts the call time in half, and the dynamic equations reduce call time by 32%. In fact, the simulation of the simplified QRTA spends less time calling a program at the cost of accuracy due to the reduction of the system states in the augmented UKF. Therefore, the simplified QRTA has been proved to be employed effectively in practice for time-limited alignment, although the full-information QRTA has a more accurate alignment result.

C. THE POLAR-REGION DATA GENERATIONS FOR THE SEMI-PHYSICAL EXPERIMENTS

In practice, the data sensed by gyros and accelerometers can be modeled as follows:

$$\hat{f}^b = f^b + \nabla^b$$
$$\hat{\omega}_{ib}^b = \omega_{ib}^b + \varepsilon^b,$$

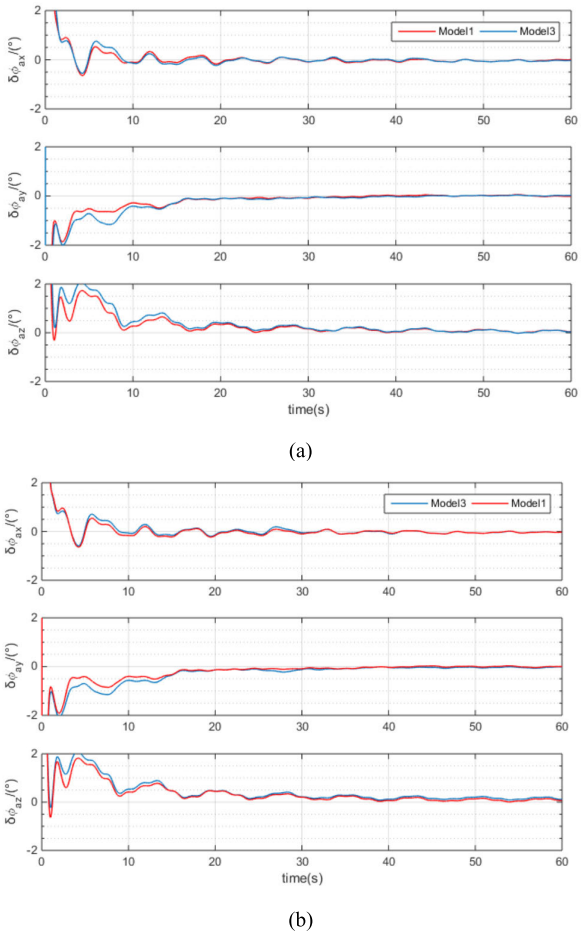

FIGURE 3. Attitude estimate error curves of ϕ_a^G in the moderate sea conditions with different lever-arm lengths for various models. (a) with the lever-arm length of 1m, 2m, and 2m; (b) with the lever-arm length of 15m, 10m, and 45m.

where the superscript b represents the body frame, referring to the master and slave body frame. The practical inertial measurements (i.e., $\hat{f}^b$ and $\hat{\omega}_{ib}^b$) are composed of the true data (i.e., f^b and ω_{ib}^b) and its errors (i.e., accelerometer bias ∇^b and gyro drift ε^b).

Provided by the confirmed latitudes and maneuvers, the real data are the same no matter where the data is obtained. Thereby, the values of f^b and ω_{ib}^b can be determined via the trajectory generator and simulation. As follows in Fig.4, the IMU-based SDINS comprises the 3-axis accelerometers and gyros, fixed on a high-precision turntable, and supplies rotary movements. The errors can be extracted from the measured data of the IMU. Thus, the real data via simulations plus the errors obtained from the non-polar data generates the semi-physical experimental data of polar regions through the lab-based experiments.

After the lab-based experiment, the constant drifts of the 3-axis gyros are $-3.6245 \times 10^{-9} rad/s$, $9.8537 \times 10^{-9} rad/s$, and $-9.6793 \times 10^{-8} rad/s$ with random variances of $\left(3.324 \times 10^{-6} rad/s\right)^2$, $\left(3.76 \times 10^{-6} rad/s\right)^2$,

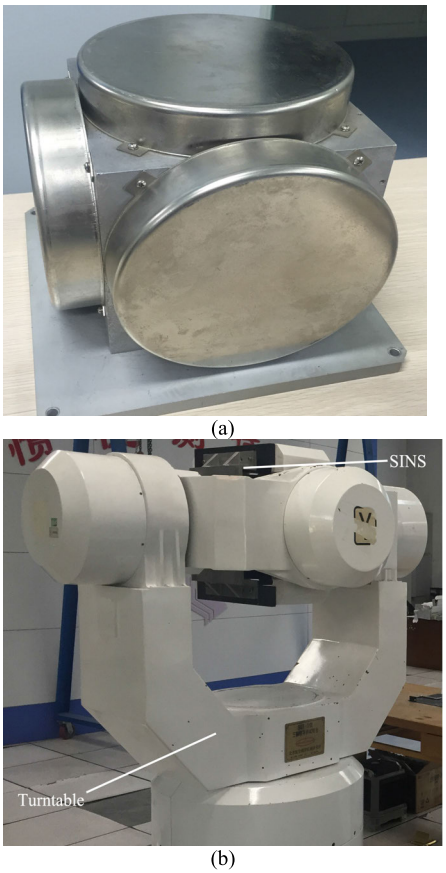

(a)

(b)

FIGURE 4. Experimental device (a) IMU; (b) the turntable and SINS.

and $\left(1.449 \times 10^{-6} rad/s\right)^2$. The constant bias of the 3-axis accelerometers are $-8.9071 \times 10^{-6} m/s^2, 6.5986 \times 10^{-6} m/s^2$, and $-3.8755 \times 10^{-6} m/s^2$ with random variances of $\left(0.001809\, m/s^2\right)^2$, $\left(0.001358 m/s^2\right)^2$, and $\left(0.0003836 m/s^2\right)^2$.

D. SEMI-PHYSICAL EXPERIMENT RESULTS AND DISCUSSIONS

Other conditions can be referred in Section IV-A. Semi-physical experiment results of Model 1 and Model 2 under the three typical maneuvers in the moderate sea conditions are shown in Fig.5 and Table 3 with misalignment angles of 15°, 15°, and 60°.

As shown in Fig.5 and Table 3, semi-physical experiment results further verify that Model 1 performs better than Model 2 on both accuracy and convergence speed. Model 1 even restrains the alignment time within 5 seconds. This merit results from the option of the attitude rotation quaternion in the grid frame, which is applied as the full-orientation attitude representation in the polar RTA algorithm. The time slippage for convergence is that attitude rotation quaternion rotates the frame once from one to another. In contrast, Euler angel represents a time-consuming transformation using a three-time successive rotation in a sequence.

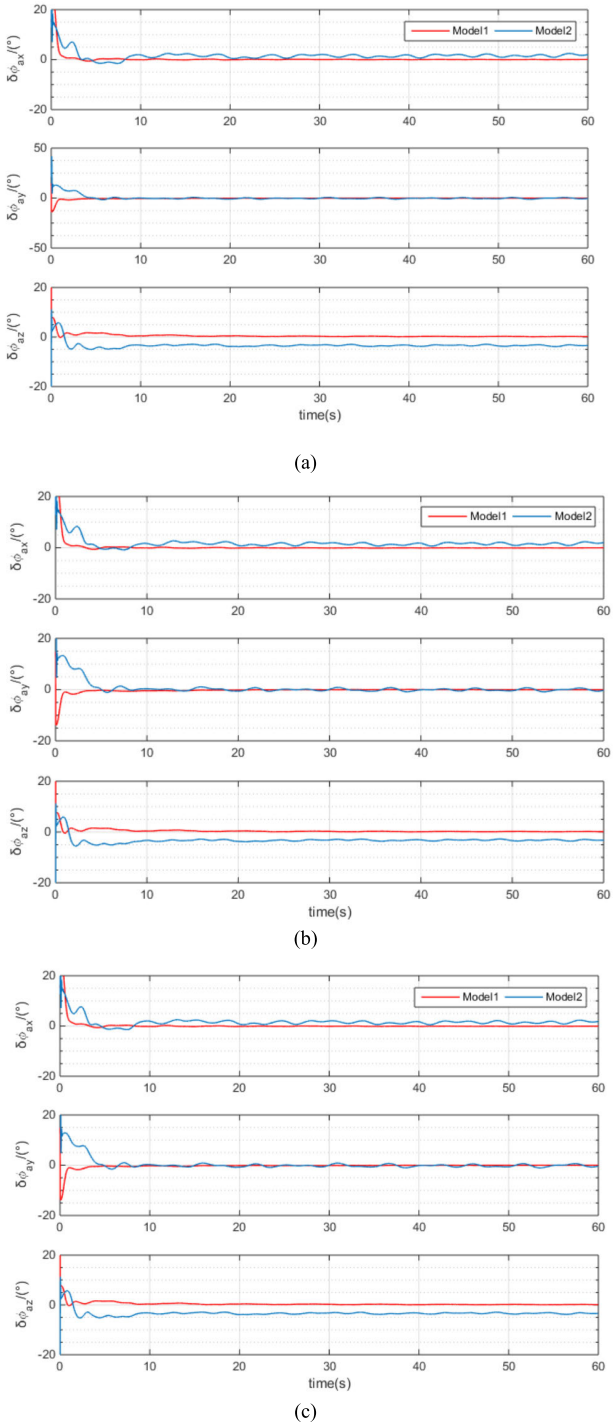

(a)

(b)

(c)

FIGURE 5. Attitude estimate error curves of ϕ_a^G in medium sea state and semi-physical experiments (a) in the static motion; (b) in the uniform linear motion; (c) in the uniformly accelerated motion.

Semi-physical experiment results of Model 1 and Model 3 under the three typical maneuvers in the moderate sea conditions are shown in Fig.6 and Table 4 with misalignment angles of 15°, 15°, and 60°.

With the lever-arm length of 1m, 2m, and 2m, the 3-axis angle misalignment of Model 1 reduces by 0.0064°,

TABLE 3. RMS errors of RTA in the medium sea state and semi-physical experiments.

Parameters	Model	The static motion	The uniform linear motion	The uniformly accelerated motion
Pitch /(°)	Model 1	0.0429	0.0888	0.0973
	Model 2	1.6124	1.6218	1.4936
Roll /(°)	Model 1	0.0704	0.0246	0.0545
	Model 2	0.5406	0.5213	0.5116
Yaw /(°)	Model 1	0.2207	0.1755	0.1754
	Model 2	3.4204	3.4049	3.3727

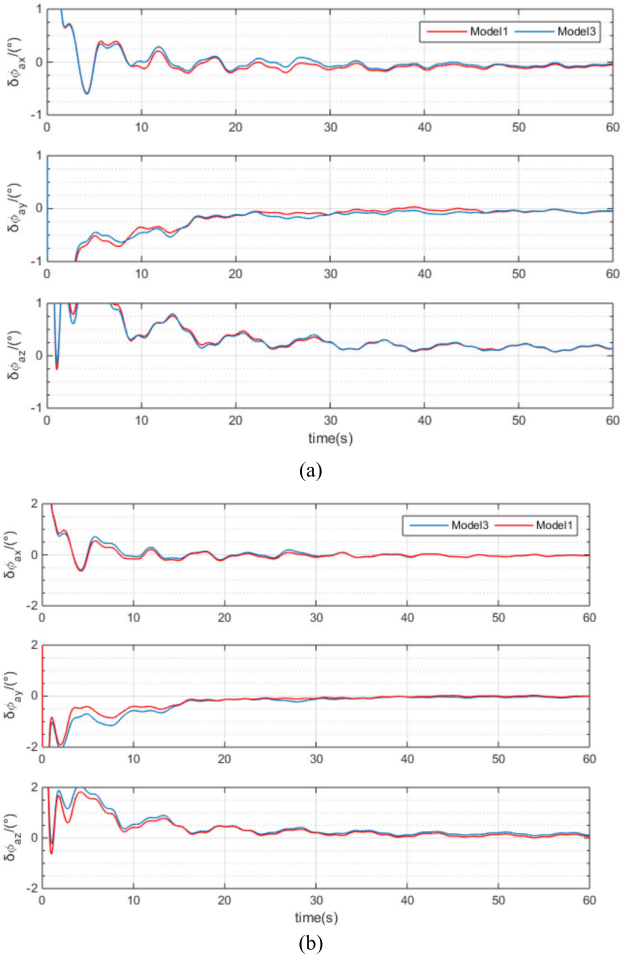

FIGURE 6. Attitude estimate error curves of ϕ_a^G in the medium sea conditions and semi-physical experiments. (a) with the lever-arm length of 1m, 2m, and 2m; (b) with the lever-arm length of 15m, 10m, and 45m.

-0.0064°, and -0.0086° over that of Model 3. With the lever-arm length of 15m, 10m, and 40m, the 3-axis angle misalignment of Model 1 reduces by 0.0021°, 0.0005°, and 0.0053° over that of Model 3. Thus, semi-physical experiment results

TABLE 4. RMS errors of RTA with various lever-arm length in semi-physical experiments.

Parameters	Model	Lever arm: 1m-2m-2m	Lever arm: 15m-10m-40m
Pitch /(°)	Model 1	0.0445	0.0805
	Model3	0.0509	0.0826
Roll /(°)	Model 1	0.0752	0.0668
	Model 3	0.0688	0.0673
Yaw /(°)	Model 1	0.1871	0.1803
	Model 3	0.1785	0.1856

in Fig.6 and Table 4 proves that the attitude rotation quaternion can anti-interfere the lever-arm effect induced by the extreme state of the sea in polar regions.

The semi-physical experiment results imply that Algorithm 1 enables the shipborne SINS to align and work effectively in polar regions. Furthermore, the polar rapid transfer alignment based on the quaternion matching and the augmented UKF can perform accurately in the case of the 3-axis large misalignments and has superior robustness for the disturbance of the lever arm.

V. DISCUSSION

As shown in the simulation and semi-physical experiment results, the innovative polar RTA algorithm using the quaternion matching method and the augmented UKF is significantly superior to the traditional polar RTA algorithms for 3-axis large attitude misalignments. Compared with traditional ones, the novel algorithm proposed in this article possesses below merits: (1) The traditional algorithms of polar RTA assume the horizontal attitude errors as small angles to derive the linear relation between the rotation rates $\omega_{ms'}^{s}$ and the angular velocity of ϕ_m^G. So, the conventional nonlinear model merely suits a large azimuth misalignment. When the horizontal attitude errors increase, the traditional algorithms may magnify RMS error or even diverge in results. Since the quaternion is an all-orientation attitude representation without any singularity during rotation, the attitude kinematics based on the misalignment quaternion propagate and evolve in time under no angle approximation assumptions. The differential equation can then estimate the physical angle errors for 3-axis large attitude misalignments. Besides, the transformation rotates the matrix once by the quaternion, rather than 3 times via the Euler angle algorithm. Model 1 thereby spends less time on converging than Model 2.

(2) The lever-arm effect is a theoretical error caused by the distance among systems. Adding this error as a master velocity error may introduce the distortion into the system. Thus, calculation compensation is customarily adopted, which augments the lever-arm length into systematic states,

estimates, and then compensates directly. There are two models constructed for the augmented UKF in this article. One is a full-information model for QRTA as Algorithm 1, in which the state and measurement models consider the lever-arm compensation. Another is a simplified model as Algorithm 2, which omits all associated lever-arm terms and increases the process noise to offset. The full-information algorithm is straightforward and high-precision, yet it evolves complicatedly and compensates hardly online. According to the results in the simplified QRTA, the multiplicative attitude rotation quaternion is barely sensitive to the error rendered via the lever-are effect. The call time of the main program in Model 3 also costs less than Model 1, since the number of system states for UKF decrease. Therefore, as far as the residual for incomplete lever-arm compensation occurs, the multiplicative misalignment quaternion is advised to be employed as the state and observation to construct the polar RTA model. Furthermore, as far as the accuracy is allowed, the simplified QRTA algorithm can also be adopted as an alternative of full-information QRTA for a time-saving transfer alignment.

VI. CONCLUSION

In the case of divergence and singularity of 3-axis large-angle misalignments occurring in the traditional polar RTA algorithm, an innovative polar rapid transfer alignment, using the quaternion matching method and the augmented UKF, is proposed here for arbitrary misalignments. In this article, the proposed algorithm adopts the misalignment quaternion in the grid frame as the state and observation to rederive quaternion-based mathematic system models for polar RTA. The quaternion matching method solves the 3-axis large-angle misalignments, decreases the model nonlinearity, and makes the measurement equation more linear. Additionally, we adjust the augmented UKF and apply it to process the non-additive noise coupled by quaternion multiplication. Simulation and semi-physical experiment results have demonstrated that, in the case of 3-axis large attitude errors, the polar QRTA proposed in this article is superior to the traditional RTA. Furthermore, the comparison of Model 1 and Model 3 shows that the proposed algorithm is barely disturbed by the lever-arm effect. Since the lever-arm effect frequently occurs in the severe environment of polar regions, the polar rapid transfer alignment based on quaternion error is superior to the traditional ones matched by Euler angles in the robustness of lever-arm disturbance. Thus, the polar rapid transfer alignment proposed in this article has better feasibility for the 3-axis large misalignments, owns great superiority for lever-arm disturbance, and can be widely used in the field of Engineering of polar regions.

REFERENCES

[1] R. McEwen, H. Thomas, D. Weber, and F. Psota, "Performance of an AUV navigation system at arctic latitudes," *IEEE J. Ocean. Eng.*, vol. 30, no. 2, pp. 443–454, Apr. 2005.

[2] J. Cheng and J. Cai, "Navigation of polar vessel," in *Encyclopedia of Ocean Engineering*, W. Cui, S. Fu, and Z. Hu, Eds. Singapore: Springer, 2020.

[3] J. Zhou, X. Nie, and J. Lin, "A novel laser Doppler velocimeter and its integrated navigation system with strapdown inertial navigation," *Opt. Laser Technol.*, vol. 64, pp. 319–323, Dec. 2014.

[4] G. Chen, K. Li, W. Wang, and P. Li, "A novel redundant INS based on triple rotary inertial measurement units," *Meas. Sci. Technol.*, vol. 27, no. 10, Oct. 2016, Art. no. 105102.

[5] J. Kain and J. Cloutier, "Rapid transfer alignment for tactical weapon applications," in *Proc. Guid., Navigat. Control Conf.*, 1991, p. 3581.

[6] C. C. Ross and T. F. Elbert, "A transfer alignment algorithm study based on actual flight test data from a tactical air-to-ground weapon launch," in *Proc. IEEE Position, Location Navigat. Symp. (PLANS)*, 2002, pp. 431–438.

[7] W. Huang, T. Fang, L. Luo, L. Zhao, and F. Che, "A damping grid strapdown inertial navigation system based on a Kalman filter for ships in polar regions," *Sensors*, vol. 17, no. 7, p. 1551, Jul. 2017.

[8] E. Bekir, *Introduction to Modern Navigation Systems*. Singapore: World Scientific, 2007.

[9] F. Wu, Y. Y. Qin, and Q. Zhou, "Airborne weapon transfer alignment algorithm in polar regions," *J. Chin. Inertial Technol.*, vol. 21, no. 2, pp. 1141–1713, 2013.

[10] Q. Zhou, Y. Qin, Q. Fu, and Y. Yue, "Grid mechanization in inertial navigation systems for transpolar aircraft," *J. Northwestern Polytech. Univ.*, vol. 31, no. 2, pp. 210–217, Apr. 2013.

[11] X. Y. Kong, E. M. Nebot, and H. Durrant-Whyte, "Development of a non-linear psi-angle model for large misalignment errors and its application in INS alignment and calibration," in *Proc. IEEE Int. Conf. Robot. Automat.*, Detroit, MI, USA, May 1999, pp. 1430–1435.

[12] J. Cheng, T. Wang, D. Guan, and M. Li, "Polar transfer alignment of shipborne SINS with a large misalignment angle," *Meas. Sci. Technol.*, vol. 27, no. 3, Mar. 2016, Art. no. 035101.

[13] C. L. Wei, H. Y. Zhang, and S. G. Hao, "SINS nonlinear alignment with large azimuth misalignment angles," *Aerosp. Control*, vol. 21, no. 4, pp. 25–35, 2003.

[14] X. Cui, G. Yan, Q. Fu, Q. Zhou, and Z. Liu, "A unified nonsingular rapid transfer alignment solution for tactical weapon based on matrix Kalman filter," *IEEE Access*, vol. 6, pp. 78700–78709, 2018.

[15] Z.-Q. Wang *et al.*, "Transfer alignment of shipborne aircraft with large misalignment based on rotation vector error model," *Zhongguo Guanxing Jishu Xuebao/J. Chin. Inertial Technol.*, vol. 24, no. 6, pp. 723–729, Dec. 2016.

[16] X. Kong, "INS algorithm using quaternion model for low cost IMU," *Robot. Auto. Syst.*, vol. 46, no. 4, pp. 221–246, Apr. 2004.

[17] Z. L. Xiong, Y. L. Hao, and F. Sun, "Rapid matching alignment algorithm of inertial navigation system based on quaternion," *Harbin Gongcheng Daxue Xuebao/J. Harbin Eng. Univ.*, vol. 29, no. 1, pp. 28–34, 2008.

[18] H. D. Dai, S. L. Zhou, M. Chen, J. Li, and X. N. Wu, "Quaternion based nonlinear error model for rapid transfer alignment," *J. Astronaut.*, vol. 31, no. 10, pp. 2328–2334, 2010.

[19] H. Dai, S. Dai, Y. Cong, G. Zhao, and G. Wu, "Rapid transfer alignment of laser SINS using quaternion based angular measurement," *Optik*, vol. 124, no. 20, pp. 4364–4368, Oct. 2013.

[20] M.-J. Yu, J. Gyu Lee, and H.-W. Park, "Comparison of SDINS in-flight alignment using equivalent error models," *IEEE Trans. Aerosp. Electron. Syst.*, vol. 35, no. 3, pp. 1046–1054, Jul. 1999.

[21] J. Cai, J. Cheng, and S. Zhong, "An innovative polar rapid transfer alignment aided by Doppler velocity log for marine vessels," in *Proc. Eur. Navigat. Conf. (ENC)*, Apr. 2019, pp. 1–8.

[22] J. L. Crassidis and F. L. Markley, "Unscented filtering for spacecraft attitude estimation," *J. Guid., Control, Dyn.*, vol. 26, no. 4, pp. 536–542, Jul. 2003.

[23] Y. Hao, Z. Xiong, W. Wang, and F. Sun, "Rapid transfer alignment based on unscented Kalman filter," in *Proc. Amer. Control Conf.*, 2006, p. 6.

[24] S. J. Julier and J. J. LaViola, "On Kalman filtering with nonlinear equality constraints," *IEEE Trans. Signal Process.*, vol. 55, no. 6, pp. 2774–2784, Jun. 2007, doi: 10.1109/TSP.2007.893949.

[25] H. Himberg and Y. Motai, "Head orientation prediction: Delta quaternions versus quaternions," *IEEE Trans. Syst., Man, Cybern., B, Cybern.*, vol. 39, no. 6, pp. 1382–1392, Dec. 2009.

[26] J. Cheng, T. Wang, L. Wang, and Z. Wang, "A new polar transfer alignment algorithm with the aid of a star sensor and based on an adaptive unscented Kalman filter," *Sensors*, vol. 17, no. 10, p. 2417, Oct. 2017.

[27] S. Gao, Y. Zhong, X. Zhang, and B. Shirinzadeh, "Multi-sensor optimal data fusion for INS/GPS/SAR integrated navigation system," *Aerosp. Sci. Technol.*, vol. 13, nos. 4–5, pp. 232–237, Jun. 2009.

[28] A. B. Younes, J. Turner, M. Majji, and J. Junkins, "Nonlinear tracking control of maneuvering rigid spacecraft," in *Proc. 21st AAS/AIAA Space Flight Mech. Meeting Adv. Astron. Sci.*, vol. 140. Escondido, CA, USA: Univelt Inc., Feb. 2011, pp. 965–981.
[29] Y. Hao, Z. Xiong, W. Wang, and F. Sun, "Rapid transfer alignment based on unscented Kalman filter," in *Proc. Amer. Control Conf.*, 2006, p. 6.
[30] Y. Wu, D. Hu, M. Wu, and X. Hu, "A numerical-integration perspective on Gaussian filters," *IEEE Trans. Signal Process.*, vol. 54, no. 8, pp. 2910–2921, Aug. 2006.
[31] X. Lu, S. Jian, and L. Haitao, "Research on matching accuracy of underwater terrain matching algorithm based on state augmented unscented Kalman filter," in *Proc. 3rd Int. Conf. Robot. Autom. Sci. (ICRAS)*, Jun. 2019, pp. 107–111.

JIANHUA CHENG is currently a Professor with the College of Intelligent Systems Science and Engineering, Harbin Engineering University, China. His current research interests include SINS and integration technology.

JING CAI is currently pursuing the Ph.D. degree with the College of Intelligent Systems Science and Engineering, Harbin Engineering University, China. Her current research interests include SINS and applications in polar regions.

ZHENMIN WANG is currently pursuing the Ph.D. degree with the College of Intelligent Systems Science and Engineering, Harbin Engineering University, China. His current research interests include SINS, polarized-light navigation, and integration technology.

JIAXIN LIU is currently pursuing the Ph.D. degree with the College of Intelligent Systems Science and Engineering, Harbin Engineering University, China. His current research interests include SINS and applications in polar regions.